Ligand Influences on the Structures of Molybdenum Oxide Networks

Pamela J. Hagrman,[†] Robert L. LaDuca, Jr.,[‡] H.-J. Koo,[§] Randy Rarig, Jr.,[†] Robert C. Haushalter,[||] Myung-Hwan Whangbo,*[,§] and Jon Zubieta*[,†]

Department of Chemistry and Physics, King's College, Wilkes-Barre, Pennsylvania 18711, Department of Chemistry, Syracuse University, Syracuse, New York 13244, General Electric Corporation Research and Development, Schenectady, New York 12301, and Department of Chemistry, North Carolina State University, Raleigh, North Carolina 27695-8204

Received May 9, 2000

The influence of organonitrogen ligands on the network structure of molybdenum oxides was examined by preparing three new molybdenum oxide phases $[MoO_3(4,4'\text{-bpy})_{0.5}]$ (MOXI-8), $[H_xMoO_3(4,4'\text{-bpy})_{0.5}]$ (MOXI-9), and $[MoO_3(\text{triazole})_{0.5}]$ (MOXI-32). The structure of $[MoO_3(4,4'\text{-bpy})_{0.5}]$ consists of layers of corner-sharing MoO_5N octahedra, buttressed by bridging 4,4′-bipyridyl ligands into a three-dimensional covalently bonded organic−inorganic composite material. Partial reduction of $[MoO_3(4,4'\text{-bpy})_{0.5}]$ yields the mixed-valence material $[H_xMoO_3(4,4'\text{-bpy})_{0.5}]$ ($x \approx 0.5$). The most apparent structural change upon reduction is found in the Mo−ligand bond lengths of the MoO_5N octahedra, which exhibit the usual (2 + 2 + 2) pattern in $[MoO_3(4,4'\text{-bpy})_{0.5}]$ and a more regular (5 + 1) pattern in $[H_xMoO_3(4,4'\text{-bpy})_{0.5}]$. Substitution of triazole for 4,4′-bipyridine yields $[MoO_3(\text{triazole})_{0.5}]$, which retains the layer motif of corner-sharing MoO_5N octahedra but with distinct sinusoidal ruffling in contrast to planar layers of $[MoO_3(4,4'\text{-bpy})_{0.5}]$ and $[H_xMoO_3(4,4'\text{-bpy})_{0.5}]$. The folding reflects the ligand constraints imposed by the triazole ligand that bridges adjacent Mo sites within a layer. MOXI-8, $C_5H_4NMoO_3$: monoclinic $P2_1/c$, $a = 7.5727(6)$ Å, $b = 7.3675(7)$ Å, $c = 22.433(3)$ Å, $\beta = 90.396(8)°$, $Z = 8$. MOXI-9, $C_5H_{4.5}NMoO_3$: monoclinic $I2/m$, $a = 5.2644(4)$ Å, $b = 5.2642(4)$ Å, $c = 22.730(2)$ Å, $\beta = 90.035(1)°$, $Z = 4$. MOXI-32, $C_2H_3N_3Mo_2O_6$: orthorhombic $Pbcm$, $a = 3.9289(5)$ Å, $b = 13.850(2)$ Å, $c = 13.366(2)$ Å, $Z = 4$.

1. Introduction

Metal oxide based solid phases are among the inorganic materials enjoying widespread interest in contemporary solid-state chemistry. Layered inorganic oxide materials are of particular interest because these materials find application in catalysis, sorption, molecular electronics, energy storage, optical materials, and ceramics.[1,2] While many of these solids are noted for their unique characteristic of allowing a wide variety of organic or inorganic chemistries to be performed in the interlamellar region, the closed-shell, diamagnetic metal oxide layers serve mainly as an inert nanoscale scaffolding. Since the processes involved in the assembly of extended inorganic solids are not fully understood, the evolution of metal oxide chemistry remains critically dependent on the synthesis of new materials possessing unique structures and properties.[3] While the synthesis of these materials remains a challenge,[4,5] the techniques of hydrothermal synthesis, in combination with the structure directing properties of organic components, may be exploited in the isolation of metastable inorganic−organic composites that retain the structural elements of the synthetic precursors.[6,7] The cooperative assembly of metal oxide−organic phases has been demonstrated by the recent reports of novel one-dimensional molybdenum oxide polymers, incorporating organoammonium cations [8,9] or organonitrogen ligands directly coordinated to the oxide substructure,[10] as well as two-dimensional materials based on molybdenum oxide layers with organic groups occupying the interlamellar regions[11,12] and based on bimetallic oxide compositions exhibiting integral organic ligation.[13] There also exist a number of lamellar vanadium oxide solids that have been prepared by the intercalation of alkali metal cations,[14] conductive organic polymers,[15] and organic cations[16] between the layers of V_2O_5. Our research has demonstrated that not only does the $V_2O_5 \cdot nH_2O$ host of these materials possess a porous layered structure capable of intercalating various neutral and charged

[†] Syracuse University.
[‡] King's College.
[§] North Carolina State University.
[||] General Electric Corporation Research and Development.

(1) Cheetham, A. J. *Science* **1994**, *264*, 794 and references therein.
(2) Cox, P. A. *Transition Metal Oxides*; Clarendon Press: Oxford, England, 1995.
(3) Bhuvanesh, N. S. P.; Prasad, B. R.; Subramanian, C. K.; Gopalakrishnan, J. *Chem. Commun.* **1996**, 289.
(4) Stein, A.; Keller, S.; Mallouk, T. E. *Science* **1993**, *259*, 1558.
(5) DiSalvo, F. J. *Science* **1990**, *247*, 649.
(6) Gopalakrishnan, J. *Chem. Mater.* **1995**, *7*, 1265.
(7) Hagrman, P.; Hagrman, D.; Zubieta, J. *Angew. Chem., Int. Ed. Engl.* **1999,** *38*, 2638.
(8) Khan, M. I.; Chen, Q.; Zubieta, J. *Inorg. Chim. Acta* **1993**, *213*, 328.
(9) Xu, Y.; An, L.-H.; Koh, L.-L. *Chem. Mater.* **1996**, *8*, 814.
(10) (a) Zapf, P. J.; Haushalter, R. C.; Zubieta, J. *Chem. Mater.* **1997**, *9*. 2019. (b) Zapf, P. J.; LaDuca, R. L., Jr.; Rarig, R. S., Jr.; Johnson, K. M., III; Zubieta, J. *Inorg. Chem.* **1998**, *37*, 3411. (c) Zapf, P. J.; Warren, C. J.; Haushalter, R. C.; Zubieta, J. *Chem. Commun.* **1997**, 1543. (d) Hagrman, D.; Zubieta, C.; Rose, D. J.; Zubieta, J. *Angew. Chem., Int. Ed. Engl.* **1997**, *36*, 795. (e) Hagrman, D.; Zubieta, J. *Chem. Commun.* **1998**, 2005. (f) Zapf, P. J.; Hammond, R. P.; Haushalter, R. C.; Zubieta, J. *Chem. Mater.* **1998**, *10*, 1336.
(11) Zapf, P. J.; Haushalter, R. C.; Zubieta, J. *Chem. Commun.* **1997**, 321.
(12) (a) Johnson, J. W.; Jacobson, A. J.; Rich, S. M.; Brody, J. F. *J. Am. Chem. Soc.* **1981**, *103*, 5246. (b) Schöllhorn, R.; Schulte-Nölle, T.; Steinhoff, G. *J. Less-Common Met.* **1980**, *71*, 71.
(13) (a) Hagrman, D.; Warren, C. J.; Haushalter, R. C.; Rarig, R. S., Jr.; Johnson, K. M., III; LaDuca, R. L., Jr.; Zubieta, J. *Chem. Mater.* **1998**, *10*, 3294. (b) Hagrman, D.; Sangregorio, C.; O'Connor, C. J.; Zubieta, J. *J. Chem. Soc., Dalton Trans.* **1998**, 3707. (c) Hagrman, D.; Zapf, P. J.; Zubieta, J. *Chem. Commun.* **1998**, 1283. (d) Hagrman, D.; Haushalter, R. C.; Zubieta, J. *Chem. Mater.* **1998**, *10*, 361.

10.1021/ic000496l CCC: $19.00
Published on Web 08/31/2000

guest species but also the incorporation of these species yields materials structurally related to V_2O_5, with the degree of reduction and condensation within the layers reflected in the charge-per-volume ratio of the interlamellar cation. Extending these ideas, we were able to prepare an entirely new class of layered, mixed-valence vanadium oxides that possess cationic interlayer transition or post transition metal coordination complexes.[17] Inspired by our successful investigations into the vanadium oxide system, we sought to explore the molybdenum oxide system. We felt that in addition to functioning as structure-directing cations or as components of complex cations, organoamines should serve as multifunctional ligands, forming an integral part of the covalent skeleton of the well-known layered structure adopted by MoO_3. Using 4,4′-bipyridine and 1,2,4-triazole, we have prepared three such molybdenum oxide systems: $[MoO_3(4,4'\text{-bpy})_{0.5}]$, $[H_xMoO_3(4,4'\text{-bpy})_{0.5}]$, and $[MoO_3(1,2,4\text{-triazole})_{0.5}]$. Herein we report the synthesis and the crystal and electronic band structures of these compounds.

2. Experimental Section

2.1. Syntheses and Spectroscopy. Syntheses were carried out in Parr acid digestion bombs with 23 mL of poly(tetrafluoroethylene) liners or in borosilicate tubes with $^5/_8$ in. outside diameter, $^3/_{32}$ in. wall thickness, and 6 in. length. $NiCl_2 \cdot 6H_2O$ was purchased from Aldrich and used without further purification. Water was distilled above 0.3 MΩ in-house using a Barnstead model 525 Biopure distilled water center.

Infrared spectra were obtained on a Perkin-Elmer 1600 series FTIR spectrometer. The UV−visible spectra were measured with an Ocean Optics S2000 fiber optic spectrometer with both quartz−halogen and deuterium sources. The effective wavelength range is 200−1000 nm.

The standard Kubelka Munk function was used to analyze the data.[18]

2.1.1. $[MoO_3(4,4'\text{-bpy})_{0.5}]$. A solution of MoO_3 (0.056 g 0.356 mmol), 4,4′-bipyridine (0.50 g, 0.34 mmol), and H_2O (6.7 g, 372 mmol) in the mole ratio 1:1:1094 was heated at 150 °C for 72 h in a borosilicate tube. Large yellow blocks of $[MoO_3(4,4'\text{-bpy})_{0.5}]$ were collected in 70% yield based on Mo. Anal. Calcd for $C_5H_4NO_3Mo$: C, 27.0; H, 1.81; N, 6.31. Found: C, 26.8; H, 1.70; N, 6.44. IR (KBr pellet, cm^{-1}): 1608-(m), 1060(m), 925(s), 809(s), 772(s,br), 670(s).

2.1.2. $[H_{0.5}MoO_3(4,4'\text{-bpy})_{0.5}]$. A solution of MoO_3(0.127 g, 0.88 mmol), Mo (2−4 μm, 0.0204 g, 0.21 mmol), 4,4′-bipyridine (0.0692 g, 0.44 mmol), and H_2O (8.011 g, 445 mmol) in the mole ratio 4:0.97:2.02:2025 was heated at 180 °C for 18 h in a Parr acid digestion bomb. Black blocks of $[H_xMoO_3(4,4'\text{-bpy})_{0.5}]$ were recovered in 50% yield based on MoO_3. Anal. Calcd for $C_5H_{4.5}NO_3Mo$: C, 27.0; H, 2.02; N, 6.29. Found: C, 26.9; H, 2.10; N, 6.11. IR (KBr pellet, cm^{-1}): 1606-(m), 1057(m), 954(s), 806(m), 628(s).

2.1.3. $[MoO_3(1,2,4\text{-triazole})_{0.5}]$. A solution of Na_2MoO_4 (0.0734 g, 0.36 mmol), 1,2,4-triazole (0.0200 g, 0.29 mmol), $NiCl_2 \cdot 6H_2O$ (0.1422 g, 0.60 mmol), and H_2O (8.001 g, 444.5 mmol) in the mole ratio 1:0.95:1.67:1465 was heated for 136 h at 200 °C. Light-yellow blocks of $[MoO_3(triazole)_{0.5}]$ were recovered in ca. 74% yield based on molybdenum.

Table 1. Summary of Crystallographic Data for the Structures of $[MoO_3(4,4'\text{-bpy})_{0.5}]$ (MOXI-8), $[H_xMoO_3(4,4'\text{-bpy})_{0.5}]$ (MOXI-9), and $[MoO_3(1,2,4\text{-triazole})_{0.5}]$ (MOXI-32)

	MOXI-8	MOXI-9	MOXI-32
empirical formula	$C_5H_4NMoO_3$	$C_5H_{4.5}NMoO_3$	$C_2H_3N_3Mo_2O_6$
fw	222.03	222.54	356.95
cryst syst	monoclinic	monoclinic	orthorhombic
space group	$P2_1/c$	$I2/m$	$Pbcm$
a, Å	7.5727(6)	5.2644(4)	3.9289(5)
b, Å	7.3675(7)	5.2642(4)	13.8504(16)
c, Å	22.433(3)	22.730(2)	13.3660(15)
β, (deg)	90.396(8)	90.035(1)	
V, Å^3	1251.5(2)	629.91(8)	727.3(2)
Z	8	4	4
D_{calc}, g cm^{-3}	2.357	2.347	3.260
μ, cm^{-1}	20.28	20.18	34.53
λ, Mo Kα	0.710 73	0.710 73	0.710 73
R1[a]	0.038	0.030	0.026
wR2[b]	0.040	0.079	0.060

[a] $\sum(|F_o| - |F_c|)/\sum|F_o|$. [b] $[\sum[w(F_o^2 - F_c^2)^2]/\sum[w(F_o^2)^2]]^{1/2}$.

2.2. X-ray Crystallography. Diffraction data for $[MoO_3(4,4'\text{-bpy})_{0.5}]$ were collected on a yellow bar crystal of approximate dimensions 0.02 mm × 0.02 mm × 0.06 mm with a Rigaku AFC7R diffractometer having graphite monochromated Mo Kα radiation and an 18 kW rotating anode generator. The data were collected out to 60.1° in 2θ using the $\omega-2\theta$ scan technique at a speed of 16°/min in ω. A total of 3753 reflections were measured of which 3485 were unique (R_{int} = 0.036). The data were corrected for Lorentz and polarization effects, and an empirical absorption correction using the program DIFABS was applied (resulting in transmission factors ranging from 0.77 to 1.00). The structure was solved by direct methods using the teXsan crystallographic software package of Molecular Structure Corporation. All non-hydrogen atoms were refined anisotropically, with the hydrogen atoms themselves being included but not refined.

Crystallographic data for $[H_xMoO_3(4,4'\text{-bpy})_{0.5}]$ and $[MoO_3(triazole)_{0.5}]$ (see Table 1)were collected with a Siemens P4 diffractometer equipped with the SMART CCD system[19] and using Mo Kα radiation (λ = 0.710 73 Å). The data were collected at 100 K and corrected for Lorentz and polarization effects. Absorption corrections were made using SADABS.[20] The structure solution and refinement were carried out using the SHELXL96[21] software package. The structures were solved using direct methods, and all of the non-hydrogen atoms were located from the initial solution. After locating all of the non-hydrogen atoms in each structure, the model was refined against F^2, initially using isotropic, and later anisotropic, thermal displacement parameters until the final value of Δ/σ_{max} was less than 0.001.

The location of the proton in $[H_xMoO_3(4,4'\text{-bpy})_{0.5}]$ could not be established on the final difference Fourier maps. However, comparison of the bond valence sums[22] for the bridging oxo groups in $[H_xMoO_3(4,4'\text{-bpy})_{0.5}]$ with those for $[MoO_3(4,4'\text{-bpy})_{0.5}]$ (1.3 (av) and 1.6 (av), respectively) suggests that the proton is disordered over the bridging oxo groups of $[H_xMoO_3(4,4'\text{-bpy})_{0.5}]$. Under the synthetic conditions of this study, the value of x was approximately 0.5, as determined by elemental analyses and manganometric redox titration.[23]

(14) (a) Alkali metal cations. Liu, G.; Greendan, J. E. *J. Solid State Chem.* **1995**, *115*, 174; **1995**, *114*, 499; **1993**, *103*, 139. Bouloux, J.-C.; Galy, J. *Acta Crystallogr., Sect. B* **1973**, *29*, 1335; **1973**, *29*, 269. Murphy, D. A.; Christian, P. A.; DiSalvo, F. J.; Waszczak, J. W. *Inorg. Chem.* **1979,** *18*, 2800. (b) Organic polymer intercalates. Kanatzidis, M. J.; Wu, C.-G.; Marcy, H. O.; Kannewurf, C. R. *J. Am. Chem. Soc.* ***1989***, *111*, 4139. Kanatzidis, M. G.; Wu, C.-G.; Marcy, H. O.; DeGroot, D. G.; Kannewurf, C. R. *Chem. Mater.* **1990**, *2*, 222. Kanatzidis, M. J.; Marks, T. J. *Inorg. Chem.* **1987**, *26*, 783. (c) Organic cations. Zhang, Y.; O'Connor, C. J.; Clearfield, A.; Haushalter, R. C. *Chem. Mater.* **1996**, *8*, 595.

(15) (a) Organic polymer intercalates. Kanatzidis, M. J.; Wu, C.-G.; Marcy, H. O.; Kannewurf, C. R. *J. Am. Chem. Soc.* **1989**, *111*, 4139. (b) Kanatzidis, M. G.; Wu, C.-G.; Marcy, H. O.; DeGroot, D. G.; Kannewurf, C. R. *Chem. Mater.* **1990**, *2*, 222. (c) Kanatzidis, M. J.; Marks, T. J. *Inorg. Chem.* **1987**, *26*, 783.

(16) Organic cations. Zhang, Y.; O'Connor, C. J.; Clearfield, A.; Haushalter, R. C. *Chem. Mater.* **1996**, *8*, 595.

(17) Zhang, Y.; DeBord, J. R. D.; O'Connor, C. J.; Haushalter, R. C.; Clearfield, A.; Zubieta, J. *Angew. Chem., Int. Ed. Engl.* **1996**, *35*, 989.

(18) Kubelka, P.; Munk, F. *Z. Tech. Phys.* **1931**, *12*, 593.

(19) *Siemens SMART Software Reference Manual*; Siemens Analytical X-ray Instruments, Inc.: Madison, WI, 1994.

(20) Sheldrick, G. M. *SADABS: Program for Empirical Absorption Corrections*; University of Göttingen: Göttingen, Germany, 1996.

(21) Sheldrick, G. M. *SHELXL96. Program for the Refinement of Crystal Structures*; University of Gottingen: Göttingen, Germany, 1996.

(22) Brown, I. D. In *Structure and Bonding in Crystals*; O'Keefe, M., Navrotsky, A., Eds.; Academic Press: New York, 1981; Vol. II, p 1.

(23) Müller, A.; Krickemeyer, E.; Dillinger, S.; Bögge, M.; Plass, W.; Proust, A.; Dlocyik, L.; Menke, C.; Meyer, J.; Rohlfing, R. *Z. Anorg. Allg. Chem.* **1994**, *620*, 599.

3. Results and Discussion

3.1. Syntheses and Infrared Spectra. Hydrothermal reactions in the presence of organic molecules have been established as versatile methods for the isolation of new materials with diverse structural architectures.[24−32] While well-established for the synthesis of zeolites, the hydrothermal method has more recently been adapted to the preparation of a wide variety of metastable materials, including transition metal phosphates, polyoxoalkoxometalates, and metal oxide−ligand hybrid materials.[10] Hydrothermal reactions, typically carried out in the temperature range 120−260 °C under autogenous pressure, exploit the self-assembly of the product from soluble precursors. The reduced viscosity of water under these conditions enhances diffusion processes so that solvent extraction of solids and crystal growth from solution are favored. Since differential solubility problems arising from the mixture of organic and inorganic starting materials are minimized, a variety of simple precursors may be introduced, as well as a number of organic and/or inorganic structure-directing agents from which those of appropriate size and shape may be selected for efficient crystal packing during the crystallization process. Under such nonequilibrium crystallization conditions, metastable kinetic phases rather than the thermodynamic phase are most likely isolated. While several pathways, including the one that leads to the most stable phase, are available in such nonequilibrium mixtures, the kinetically favored structural evolution results from the smallest perturbations of atomic positions. Consequently, nucleation of a metastable phase may be favored. The general approach we have adopted is to employ an organic component at low temperature to modify or control the surface of growing composite oxide crystals in a hydrothermal medium.

The organic component of an organic−inorganic composite material may adopt a variety of roles depending on its structure, charge, and presence of heterometallic sites: (i) as a charge-compensating, space-filling, and structure-directing cation, (ii) as a ligand to a secondary transition metal center in a complex cation, and (iii) as a ligand bound directly to the inorganic matrix as a terminal group or as a pillar. In the last case, the organic ligand may associate with the primary metal constituent of the inorganic substructure or with a secondary metal site of a heterobimetallic inorganic substructure. In the present instance, the role of the organic component is that of a ligand bound directly to the molybdenum oxide framework. As discussed below, the influences of the organic component on the oxide microstructure are significant and reflect both ligand geometry and the coordination preferences of the metal.

The compound $[MoO_3(4,4'\text{-bipy})_{0.5}]$ was prepared by the hydrothermal reaction of MoO_3, 4,4′-bipyridine, and H_2O in a sealed glass tube as bright-yellow bar-shaped crystals having an overall volume significantly less than 0.1 mm^3. Crystals of $[MoO_3(4,4'\text{-bpy})_{0.5}]$ are the only solid material obtained from the reaction mixture and are isolated in approximately 70% yield.

The infrared spectrum of $[MoO_3(4,4'\text{-bpy})_{0.5}]$ exhibits ligand bands at 1608 and 1060 cm^{-1} and a strong band at 925 cm^{-1} assigned to ν(Mo═O). Strong intensity bands at 809 and 772 cm^{-1} are attributed to ν(Mo−O−Mo). The infrared spectrum of $[H_xMoO_3(4,4'\text{-bpy})_{0.5}]$ likewise exhibits ligand bands at 1606 and 1057 cm^{-1}. The ν(Mo═O) band is now at higher energy, 954 cm^{-1}, as anticipated for more reduced molybdenum sites. The bands at 806 and 628 cm^{-1} are tentatively assigned to ν(Mo−O−Mo).

3.2. Structural Characteristics. The structure of $[MoO_3(4,4'\text{-bipy})_{0.5}]$ consists of layers of corner-sharing MoO_5 square pyramids linked through 4,4′-bipyridyl groups into a three-dimensional covalently bonded metal oxide−organic ligand framework, as shown in Figure 1. The overall structure of $[MoO_3(4,4'\text{-bpy})_{0.5}]$ may be described in terms of alternating inorganic metal oxide layers and organic layers, as shown in Figure 2. The distorted MoO_5N coordination geometry at each molybdenum site is defined by a terminal oxo group, four asymmetrically bridging oxo groups, and a pyridyl nitrogen donor and has the typical "two short, two intermediate, and two long (2 + 2 + 2)" bond length geometry common to molybdenum oxides.[33] The long Mo−N distances, 2.412(6) Å on average, reflect the strong trans influence of the terminal oxo group. The terminal Mo−O bond distances of 1.698(5) Å, on average, and the bridging Mo−O bond distances, which range from 1.763(5) to 2.120(5) Å, are within the range expected for molybdenum oxides. Selected bond lengths and angles for the compound are shown in Table 2.

It should be pointed out that the structure of $[MoO_3(4,4'\text{-bpy})_{0.5}]$ is quite distinct from the layered structure adopted by MoO_3,[34] which exhibits both edge- and corner-sharing of MoO_6 octahedra. However, the $[MoO_3(4,4'\text{-bpy})_{0.5}]$ does possess the molybdenum oxide network structure proposed from powder diffraction data for the pyridine intercalation phase $[MoO_3(\text{pyridine})]$ and predicted on that basis for $[MoO_3(4,4'\text{-bpy})_{0.5}]$.[12a]

The structures of two other bipyridine-containing molybdenum(VI) oxide compounds, namely, $[MoO_3(2,2'\text{-bipy})]$[10a] and $[[H_2(4,4'\text{-bipy})][Mo_7O_{22}]\cdot H_2O]$,[11] have recently been reported. The structure of $MoO_3(2,2'\text{-bipy})$ consists of one-dimensional chains of corner-sharing MoO_4N_2 octahedra with the bipyridyl ligand serving to passivate the molybdenum oxide coordination sphere, blocking further Mo−oxo bond formation, while the structure of $[H_2(4,4'\text{-bipy})][Mo_7O_{22}]\cdot H_2O$ comprises a two-dimensional network of molybdenum oxide layers that adopt a stepped motif that is separated by an interlamellar region populated by $[H_2(4,4'\text{-bipy})]^{2+}$ cations and H_2O molecules. This particular family of compounds helps to illustrate the structural versatility of metal oxide solids, which may be realized by the introduction of organic components acting as ligands, tethers, or structure-directing cations.

As shown in Figure 3, the partially reduced phase $[H_xMoO_3(4,4'\text{-bpy})_{0.5}]$ ($x \approx 0.5$) exhibits a structure in which the characteristic network of the parent $[MoO_3(4,4'\text{-bpy})_{0.5}]$ is more or less preserved. Selected bond lengths and angles for the

(24) Haushalter, R. C.; Mundi, L. A. *Chem. Mater.* **1992**, *4*, 31−48.
(25) Khan, M. I.; Zubieta, J. *Prog. Inorg. Chem.* **1995**, *43*, 1.
(26) Khan, M. I.; Meyer, L. M.; Haushalter, R. C.; Schweitzer, C. L.; Zubieta, J.; Dye, J. L. *Chem. Mater.* **1996**, *8*, 43−53.
(27) Barrer, R. M. *Hydrothermal Chemistry of Zeolites*; Academic Press: London, 1982.
(28) Davis, M. E.; Lobo, R. F. *Chem. Mater.* **1992**, *4*, 756.
(29) Clearfield, A. *Prog. Inorg. Chem.* **1998**, *47*, 371.
(30) Loiseau, T.; Ferey, G. *J. Mater. Chem.* **1996**, *6*, 1073.
(31) Halasyamani, P. S.; Francis, R. J.; Walker, S. M.; O'Hare, D. *Inorg. Chem.* **1999**, *38*, 271 and references therein.
(32) (a) Bonavia, G. H.; Haushalter, R. C.; Lu, S.; O'Connor, C. J.; Zubieta, J. *J. Solid State Chem.* **1997**, *132*, 144. (b) Bonavia, G. H.; Haushalter, R. C.; O'Connor, C. J.; Zubieta, J. *Inorg. Chem.* **1996**, *35*, 5603. (c) Soghomonian, V.; Haushalter, R. C.; Zubieta, J. *Chem. Mater.* **1995**, *7*, 1648. (d) Soghomonian, V.; Diaz, R.; Haushalter, R. C.; O'Connor, C. J.; Zubieta, J. *Inorg. Chem.* **1995**, *34*, 4460. (e) Soghomonian, V.; Chen, Q.; Haushalter, R. C.; Zubieta, J. *Angew. Chem., Int. Ed. Engl.* **1995**, *34*, 223. (f) Khan, M. I.; Lee, Y.; O'Connor, C. J.; Haushalter, R. C.; Zubieta, J. *Inorg. Chem.* **1994**, *33*, 3855. (g) Khan, M. I.; Lee, Y.; O'Connor, C. J.; Haushalter, R. C.; Zubieta, J. *Am. Chem. Soc.* **1994**. *116*, 4525.
(33) Pope, M. T. *Heteropoly and Isopoly Oxometalates*; Springer: New York, 1983.
(34) Schröder, F. A.; Wietzel, H. *Z. Anorg. Allg. Chem.* **1977**, *435*, 247.

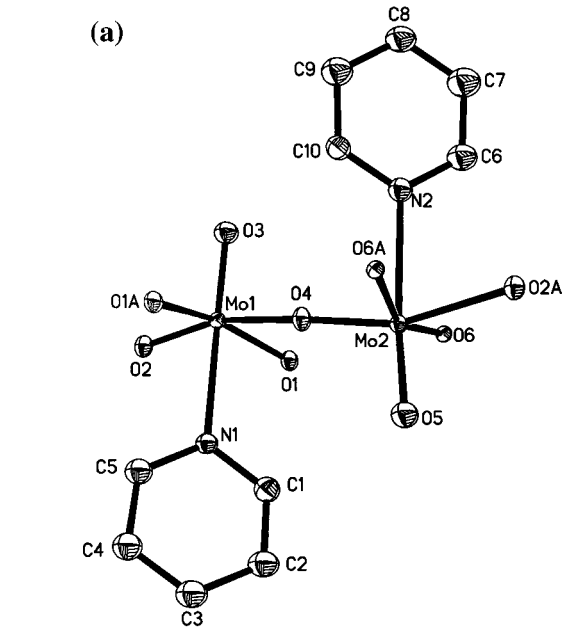

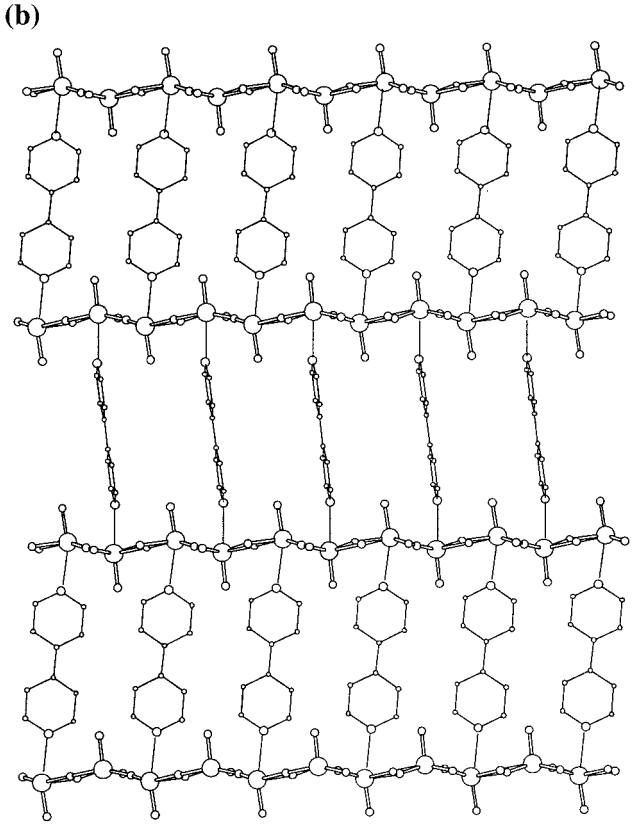

Figure 1. (a) Coordination environments of the crystallographically independent Mo sites of $[MoO_3(4,4'\text{-bpy})_{0.5}]$, showing the atom-labeling scheme and 50% thermal ellipsoids. (b) View of the layer structure of $[MoO_3(4,4'\text{-bpy})_{0.5}]$ (MOXI-8) parallel to the crystallographic *a* axis.

compound are shown in Table 3. The major structural change lies in the manner in which the MoO_5N octahedra are distorted. In $[MoO_3(4,4'\text{-bpy})_{0.5}]$, the octahedra exhibit the characteristic $2 + 2 + 2$ pattern, while in $[H_xMoO_3(4,4'\text{-bpy})_{0.5}]$, the octahedra adopt a more regular $1 + 4 + 1$ type coordination. This is similar to the structural trends observed for MoO_3 and the hydrogen-doped molybdenum oxides of general formula H_xMoO_3 ($0.02 < x < 2.0$).[35−39] The structural data for $[MoO_3(4,4'\text{-bpy})_{0.5}]$, $[H_xMoO_3(4,4'\text{-bpy})_{0.5}]$, MoO_3, and H_xMoO_3 are compared in Table 5. The structures of $[MoO_3(4,4'\text{-bpy})_{0.5}]$ and $[H_xMoO_3(4,4'\text{-bpy})_{0.5}]$ also contrast in the angles between the N···N′ axis of the bipyridyl ligands and the molybdenum oxide planes (ca. 85° and 90°, respectively) and also in the interlamellar spacing (11.22 and 11.37 Å, respectively).

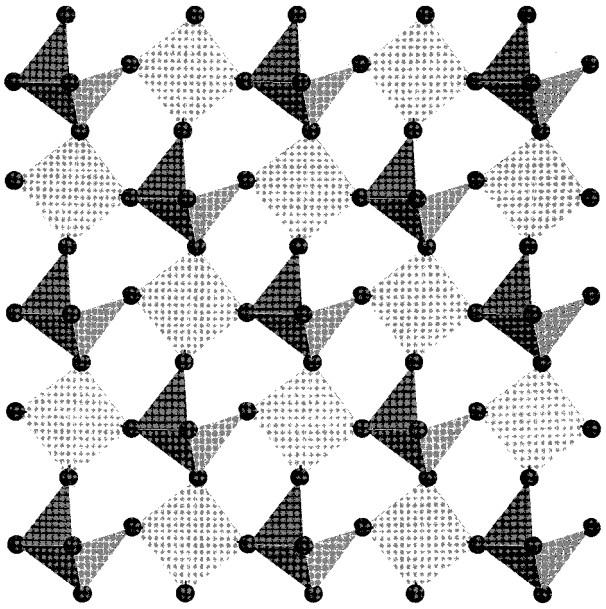

Figure 2. Polyhedral representation of the metal oxide layer of MOXI-8.

Table 2. Selected Bond Lengths (Å) and Angles (deg) for $[MoO_3(4,4'\text{-bpy})_{0.5}]$ (MOXI-8)

Mo(1)	O(1)	1.829(5)		Mo(1)	O(1)	1.985(5)	
Mo(1)	O(2)	1.763(5)		Mo(1)	O(3)	1.699(5)	
Mo(1)	O(4)	2.120(5)		Mo(1)	N(1)	2.413(6)	
Mo(2)	O(2)	2.120(5)		Mo(2)	O(4)	1.763(5)	
Mo(2)	O(5)	1.696(5)		Mo(2)	O(6)	1.810(5)	
Mo(2)	O(6)	2.006(5)		Mo(2)	N(2)	2.411(6)	
O(1)	Mo(1)	O(1)	155.51(5)	O(1)	Mo(1)	O(2)	100.2(2)
O(1)	Mo(1)	O(3)	102.1(3)	O(1)	Mo(1)	O(4)	82.5(2)
O(1)	Mo(1)	N(1)	83.3(2)	O(1)	Mo(1)	O(2)	92.8(2)
O(1)	Mo(1)	O(3)	95.1(3)	O(1)	Mo(1)	O(4)	78.7(2)
O(1)	Mo(1)	N(1)	77.6(2)	O(2)	Mo(1)	O(3)	102.7(2)
O(2)	Mo(1)	O(4)	160.7(2)	O(2)	Mo(1)	N(1)	83.9(2)
O(3)	Mo(1)	O(4)	95.3(2)	O(3)	Mo(1)	N(1)	170.4(3)
O(4)	Mo(1)	N(1)	77.5(2)	O(2)	Mo(2)	O(4)	161.1(2)
O(2)	Mo(2)	O(5)	94.3(2)	O(2)	Mo(2)	O(6)	83.6(2)
O(2)	Mo(2)	O(6)	77.4(2)	O(2)	Mo(2)	N(2)	78.0(2)
O(4)	Mo(2)	O(5)	102.8(2)	O(4)	Mo(2)	O(6)	100.3(2)
O(4)	Mo(2)	O(6)	93.1(2)	O(4)	Mo(2)	N(2)	84.9(2)
O(5)	Mo(2)	O(6)	102.5(3)	O(5)	Mo(2)	O(6)	94.3(3)
O(5)	Mo(2)	N(2)	169.5(3)	O(6)	Mo(2)	O(6)	155.47(5)
O(6)	Mo(2)	N(2)	83.8(2)	O(6)	Mo(2)	N(2)	77.2(2)
Mo(1)	O(1)	Mo(1)	161.8(3)	Mo(1)	O(2)	Mo(2)	169.8(3)
Mo(1)	O(4)	Mo(2)	156.4(3)	Mo(2)	O(6)	Mo(2)	163.0(3)

While partial reduction of the molybdenum sites retains the planar network geometry of the molybdenum oxide substructure, changes in ligand geometry may have more dramatic consequences, as observed in the structure of $[MoO_3(\text{triazole})_{0.5}]$

(35) Kihlborg, L. *Ark. Kemi* **1963**, *21*, 357.
(36) Dickens, P. G.; Birtill, J. J.; Wright, C. J. *J. Solid State Chem.* **1979**, *28*, 185.
(37) Wilhelmi, K.-A. *Acta Chem. Scand.* **1969**, *23*, 419.
(38) Adams, S.; Ehsen, K.-H.; Spilker, J. *Acta Crystallogr. B* **1993**, *49*, 958.
(39) Rousseau, R.; Canadell, E.; Alemany, P.; Galván, D. H.; Hoffmann, R. *Inorg. Chem.* **1997**, *36*, 4627.

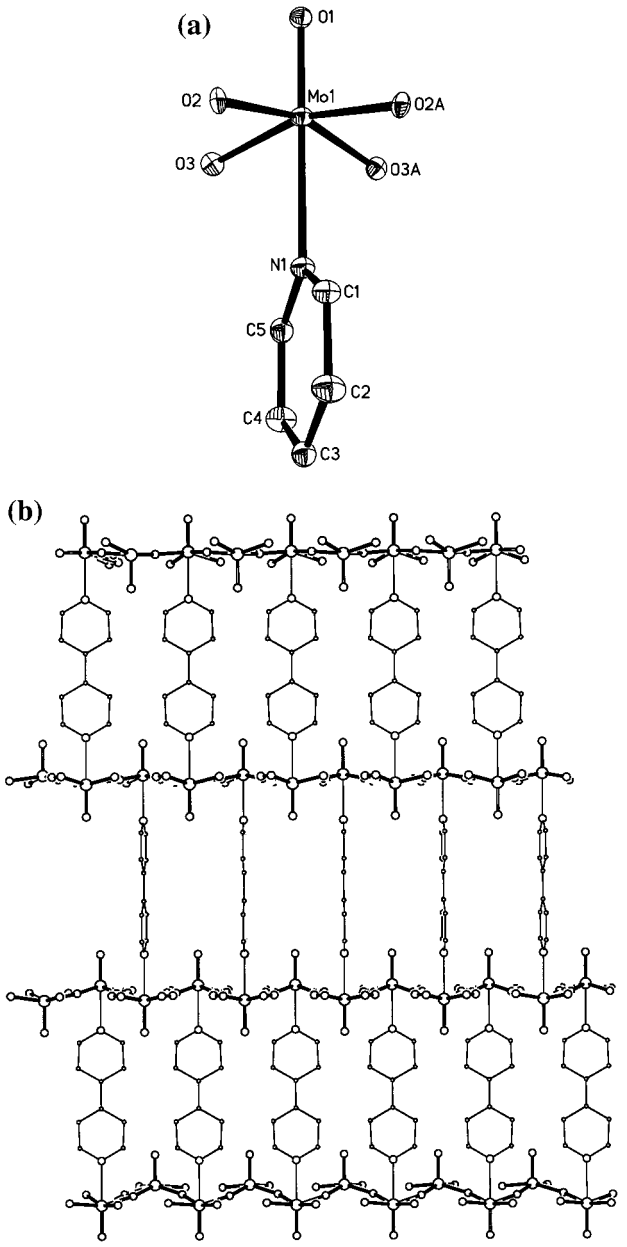

Figure 3. (a) Coordination environment of the Mo sites in $[H_xMoO_3(4,4'\text{-bpy})_{0.5}]$, showing the atom-labeling scheme and 50% thermal ellipsoids. (b) View of the buttressing of $\{H_xMoO_3\}$ layers by 4,4′-bipyridyl ligands in $[H_xMoO_3(4,4'\text{-bpy})_{0.5}]$ (MOXI-9).

Table 3. Selected Bond Lengths (Å) and Angles (deg) for $[H_xMoO_3(4,4\text{-bpy})_{0.5}]$ (MOXI-9)[a]

Mo(1)−O(1)	1.690(4)	Mo(1)−O(3)	1.922(6)
Mo(1)−O(2)#1	1.924(6)	Mo(1)−O(2)	1.929(6)
Mo(1)−O(3)#2	1.931(6)	Mo(1)−N(1)	2.445(5)
O(1)−Mo(1)−O(3)	99.4(2)	O(1)−Mo(1)−O(2)#1	99.7(2)
O(3)−Mo(1)−O(2)#1	160.9(3)	O(1)−Mo(1)−O(2)	99.8(2)
O(3)−Mo(1)−O(2)	88.5(2)	O(2)#1−Mo(1)−O(2)	88.35(7)
O(1)−Mo(1)−O(3)#2	99.8(2)	O(3)−Mo(1)−O(3)#2	88.34(8)
O(2)#1−Mo(1)−O(3)#2	88.3(2)		
O(1)−Mo(1)−N(1)	179.9(2)		
O(2)#1−Mo(1)−N(1)	80.4(2)		
O(3)#2−Mo(1)−N(1)	80.1(2)		

[a] Symmetry transformations used to generate equivalent atoms. #1: $-x + 3/2, y - 1/2, -z + 1/2$. #2: $-x + 1/2, y - 1/2, -z + 1/2$. #3: $-x + 1, -y, -z + 1$.

shown in Figure 4 with selected bond lengths and angles listed in Table 4. The structure again consists of MoO_3 networks of

Table 4. Selected Bond Lengths (Å) and Angles (deg) for $[MoO_3(1,2,4\text{-triazole})_{0.5}]$ (MOXI-32)[a]

Mo(1)−O(3)	1.700(3)	Mo(1)−O(2)	1.9288(14)
Mo(1)−O(4)	1.729(4)	Mo(1)−O(4)#1	2.224(4)
Mo(1)−O(1)	1.8931(9)	Mo(1)−N(2)	2.354(3)
O(3)−Mo(1)−O(4)	104.80(15)	O(3)−Mo(1)−N(2)	162.91(14)
O(3)−Mo(1)−O(1)	101.19(11)	O(4)−Mo(1)−N(2)	91.10(14)
O(4)−Mo(1)−O(1)	98.3(2)	O(1)−Mo(1)−N(2)	82.26(9)
O(3)−Mo(1)−O(2)	95.44(16)	O(2)−Mo(1)−N(2)	75.95(15)
O(4)−Mo(1)−O(2)	97.56(19)	O(4)#1−Mo(1)−N(2)	76.16(13)
O(1)−Mo(1)−O(2)	153.17(17)	Mo(1)−O(4)−Mo(1)#2	167.26(19)
O(3)−Mo(1)−O(4)#1	87.85(14)	Mo(1)#3−O(2)−Mo(1)	142.6(2)
O(4)−Mo(1)−O(4)#1	167.26(19)	Mo(1)#4−O(1)−Mo(1)	161.7(3)
O(1)−Mo(1)−O(4)#1	80.29(18)		
O(2)−Mo(1)−O(4)#1	79.45(17)		

[a] Symmetry transformations used to generate equivalent atoms. #1: $x - 1, y, z$. #2: $x + 1, y, z$. #3: $x, y, -z + 3/2$. #4: $x, -y + 1/2, -z + 2$.

Table 5. Comparison of Bond Lengths (Å) for the Molybdenum Oxides of This Study and Related Materials

	$Mo-O_t$	$Mo-O_{equatorial}$	$Mo-L_{axial}$	valence sums[35]
$[MoO_3(4,4'\text{-bpy})_{0.5}]$ (MOXI-8)	1.697(5), av	1.763(5) 1.820(5), av 2.001(5), av 2.120(5), av	2.412(6), av	6.10
$[H_xMoO_3(4,4'\text{-bpy})_{0.5}]$ (MOXI-9)	1.690(4)	1.922(6) 1.924(6) 1.929(6) 1.931(6)	2.445(5)	5.41
$[MoO_3]$	1.671	1.755 1.948 1.948 2.251	2.332	5.90
$[H_xMoO_3]$	1.69, av	1.95 × 4, av	2.33, av	5.14

corner-sharing octahedra, with the ligands projecting above and below the oxide layers. The most apparent structural change from the $[MoO_3(4,4'\text{-bpy})_{0.5}]$ and $[H_xMoO_3(4,4'\text{-bpy})_{0.5}]$ prototypes is the sinusoidal ruffling of molybdenum oxide networks, with an amplitude of ca. 4.1 Å and a period of ca. 13.4 Å. The distortion from planarity is a consequence of the ligation mode of the triazole ligand.

As a neutral ligand, triazole adopts a bidentate-bridging coordination mode through the 1,2-nitrogen sites. The structural consequence of this bridging mode is to tilt adjacent molybdenum octahedra such that the vertexes occupied by the nitrogen donors of the triazole ligand are pinched together while the O_4- equatorial planes and the vertexes trans to the nitrogen donors are titled away. As shown in Figure 5, the consequence is a layer structure that may be described as $[(Mo_2O_3)O_{6/2}(\text{triazole})]_n$ double chains linked through corner-sharing to the two-dimensional network. The alternation of the triazole ligand above and below the oxide plane on adjacent chains results in the observed sinusoidal ruffling.

It is noteworthy that the registry of layers positions the N−H group of the triazole of one layer directly above or below the bridging oxo group of the Mo_2O_3 grouping of the adjacent layer. This results in significant hydrogen bonding between the layers with an O···H(N) distance of 1.75 Å and an O−H−N angle of 180°.

3.3. Electronic Structure. The electronic band structures of $[MoO_3(4,4'\text{-bpy})_{0.5}]$, $[H_xMoO_3(4,4'\text{-bpy})_{0.5}]$, and $[MoO_3(\text{triazole})_{0.5}]$ were calculated using the extended Hückel method.[40−42] The total density of states (DOS) calculated for MoO_3-

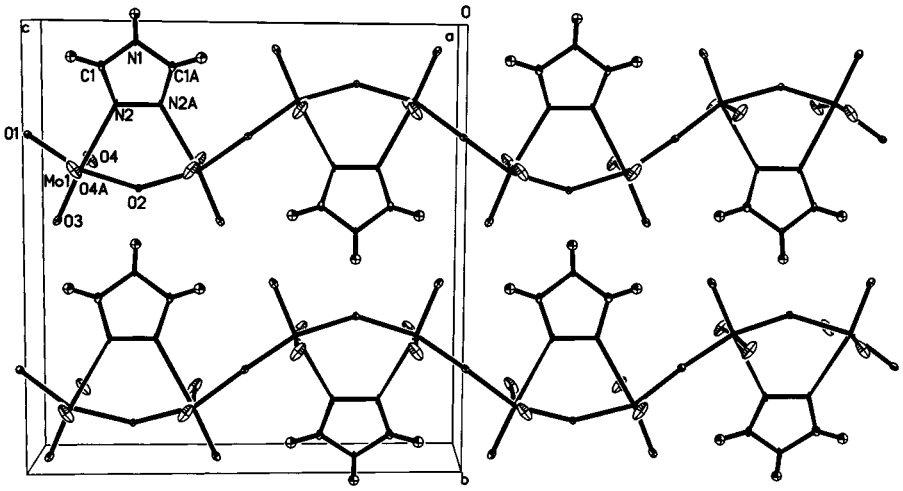

Figure 4. View parallel to the crystallographic *a* axis of the structure of $[MoO_3(1,2,4\text{-triazole})_{0.5}]$ (MOXI-32), showing the atom-labeling scheme and 50% thermal ellipsoids.

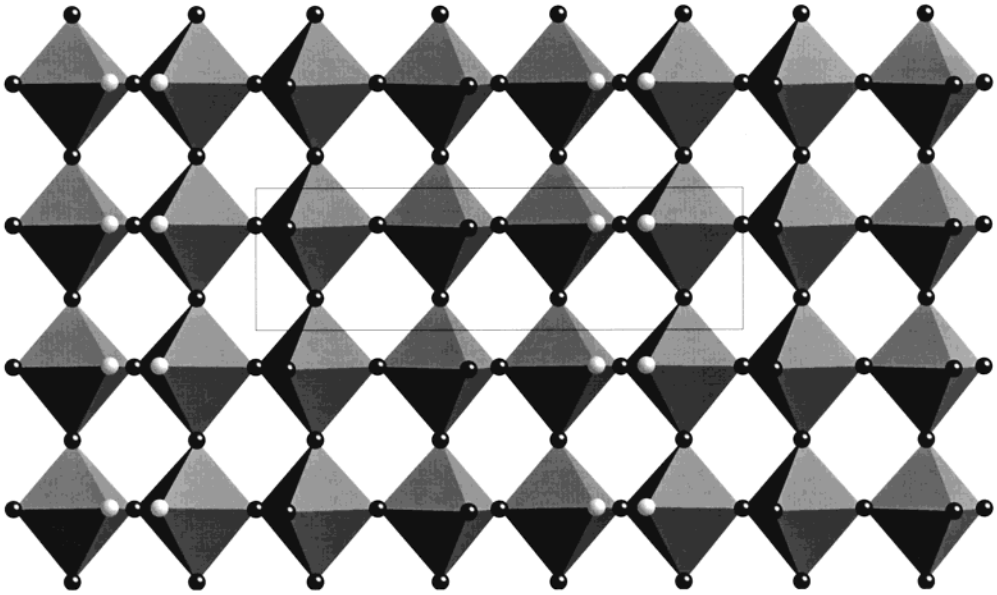

Figure 5. Polyhedral representation of the molybdenum oxide layer of MOXI-32.

$(4,4'\text{-bpy})_{0.5}$ is shown in Figure 6a, where the dotted curves represent the partial density of states (PDOS) for the Mo 4d orbitals and the dashed curves the PDOS for the O 2p orbitals. The Fermi level (vertical dashed line) lies at the HOMO of 4,4′-dipyridine, which lies in the middle of the energy gap between the p- and d-block bands of the MoO_3 framework. The LUMO of 4,4′-dipyridine is calculated to lie near the bottom of the d-block bands of the MoO_3 framework. The electronic band structure of $[H_xMoO_3(4,4'\text{-bpy})_{0.5}]$ can be approximated by that of its $[MoO_3(4,4'\text{-bpy})_{0.5}]^{x-}$ lattice. The electronic structure of the $[MoO_3(4,4'\text{-bpy})_{0.5}]^{x-}$ lattice is quite similar to that of $[MoO_3(4,4'\text{-bpy})_{0.5}]$, as shown in Figure 6b, where the Fermi level of Figure 6b is given for $x = 0.5$. The electronic band structure calculated for $[MoO_3(\text{triazole})_{0.5}]$ is presented in Figure 6c, which shows that the LUMO of triazole lies above the d-block bands of the MoO_3 framework.

To understand the optical and other physical properties of $[MoO_3(4,4'\text{-bpy})_{0.5}]$, $[H_xMoO_3(4,4'\text{-bpy})_{0.5}]$, and $[MoO_3(\text{triazole})_{0.5}]$, it is necessary to check the accuracy of the calculated energy levels of the inorganic framework relative to those of the organic ligands. Thus, we calculated the molecular electronic structures of 4,4′-dipyridine and triazole based on the extended Hückel method and also on the density functional theory using the ADF program package.[43−46] The lowest ($\pi-\pi^*$) excitation energies of 4,4′-dipyridine and triazole are calculated to be 2.75 and 4.77 eV, respectively, from the extended Hückel method, but they are 3.76 and 5.95, eV, respectively, from the density functional theory. Since 4,4′-dipyridine is colorless, the excitation energies obtained from the density functional theory are consistent with experimental results, and the extended Hückel method underestimates these energies by about

(40) Hoffmann, R. *J. Chem. Phys*. **1967**, *39*, 1397.
(41) Whangbo, M.-H.; Hoffman, R. *J. Am. Chem. Soc*. **1978**, *100*, 6397.
(42) Our calculations were carried out by employing the CAESAR program package (Ren, J.; Liang, W.; Whangbo, M.-H. *Crystal and Electronic Structure Analysis Using CAESAR*; 1998. This book can be downloaded free of charge from the web site http://www.PrimeC.com/.)
(43) *ADF*, release 1.1.3; Department of Chemistry, Vrije Universiteit: Amsterdam, 1997.
(44) Baerends, E. J.; Ellis, D. E.; Ros, P. *Chem. Phys*. **1973**, *2*, 41.
(45) te Velde, G.; Baerends, E. J. *J. Comput. Phys.* **1992**, *99*, 84.
(46) The calculations were carried out with the frozen core approximation. The orbitals of C, N, and H were represented by triple-ζ basis functions.

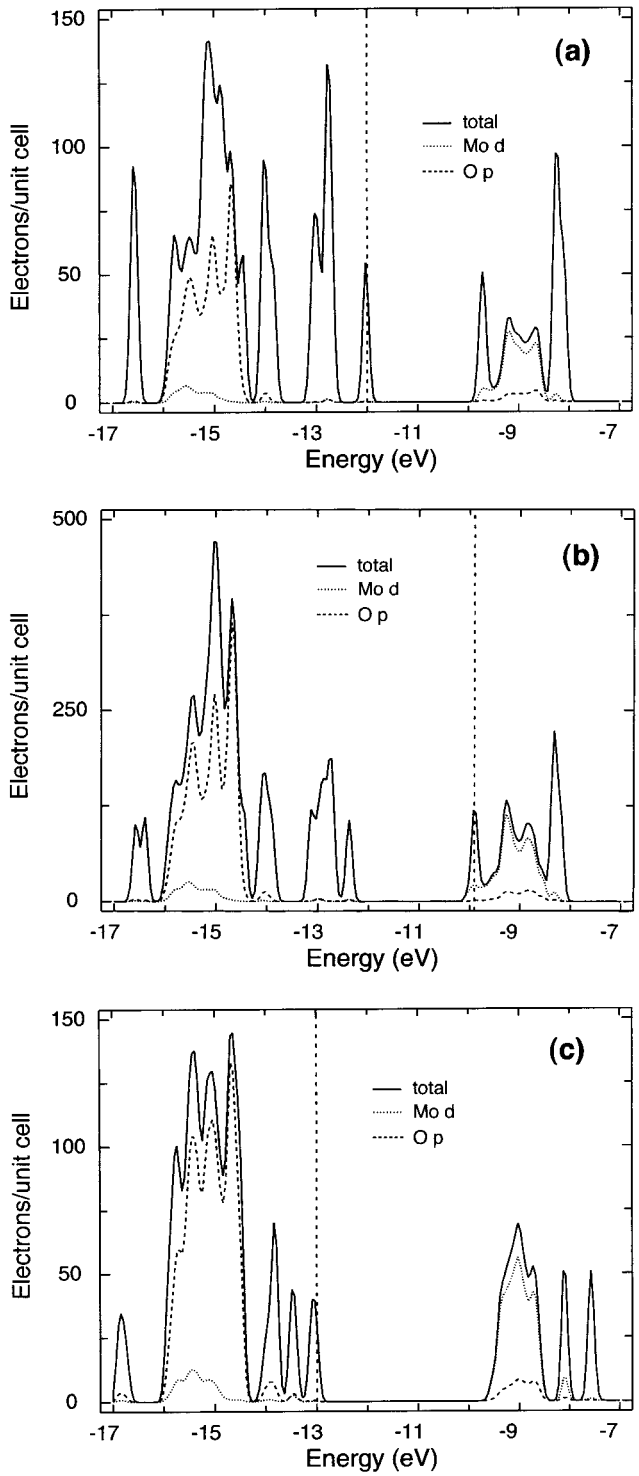

Figure 6. Electronic band structures of (a) $[MoO_3(4,4'\text{-bpy})_{0.5}]$, (b) $[H_{0.5}MoO_3(4,4'\text{-bpy})_{0.5}]$, and (c) $[MoO_3(\text{triazole})_{0.5}]$ calculated using the extended Hückel method. The unit cells of $[MoO_3(4,4'\text{-bpy})_{0.5}]$, $[H_xMoO_3(4,4'\text{-bpy})_{0.5}]$, and $[MoO_3(\text{triazole})_{0.5}]$ have 4, 16, and 8 formula units, respectively.

1 eV. The color of $[MoO_3(4,4'\text{-bpy})_{0.5}]$ is yellow, and diffuse reflectance measurements for $[MoO_3(4,4'\text{-bpy})_{0.5}]$ show a broad absorbance centered at 390 nm. This indicates that the bottom of the d-block bands of the MoO_3 framework lies approximately 2 eV above the HOMO of 4,4′-dipyridine. Therefore, the true position of the LUMO of 4,4′-dipyridine in parts a and b of Figure 6 should not be near the bottom of the d-block bands but near the middle of the d-block bands. This means that in the $[H_xMoO_3(4,4'\text{-bpy})_{0.5}]$ system, the extra electrons generated by the hydrogen doping will reside in the d-block bands, not in the LUMO of 4,4′-dipyridine. Thus, the $[H_xMoO_3(4,4'\text{-bpy})_{0.5}]$ ($x \approx 5$) system is expected to be metallic, as found for H_xMoO_3.[36] Diffuse reflectance measurements for $[H_xMoO_3(4,4'\text{-bpy})_{0.5}]$ exhibit broad absorbances at 390 and 520 nm and show no transmission above 600 nm and less than 20% transmission beyond 380 nm. The latter is consistent with the metallic character proposed.

4. Concluding Remarks

Hydrothermal synthesis has been used to prepare a series of layered organic−inorganic hybrid materials. The unique characteristics of organic and inorganic components complement each other in such hybrid materials, leading to new solid-state structures and materials with composite or even new properties.

The "pillared" layer structure of $[MoO_3(4,4'\text{-bpy})_{0.5}]$, first proposed by Jacobson and co-workers,[11] has been largely confirmed. Furthermore, exploitation of hydrothermal techniques allows isolation of the mixed-valence material $[H_xMoO_3(4,4'\text{-bpy})_{0.5}]$ ($x \approx 0.5$). Calculation of the electronic band structures of $[MoO_3(4,4'\text{-bpy})_{0.5}]$ and $[H_xMo_3(4,4'\text{-bpy})_{0.5}]$ using extended Hückel methods reveals that $[MoO_3(4,4'\text{-bpy})_{0.5}]$ is a semiconductor while $[H_xMo_3(4,4'\text{-bpy})_{0.5}]$ is metallic. This latter observation is confirmed by the diffuse reflectance properties of $[H_xMo_3(4,4'\text{-bpy})_{0.5}]$.

The structure-directing properties of the organic component are apparent in the pillared layer structures of $[MoO_3(4,4'\text{-bpy})_{0.5}]$ and $[H_xMo_3(4,4'\text{-bpy})_{0.5}]$. Modification of ligand geometry should influence the structure of the composite. Hydrothermal reactions with 1,2,4-triazole, which may assume tridentate coordination as the 1,2,4-triazolate anion, in place of 4,4′-bipyridine, yielded the undulating two-dimensional phase $[MoO_3(1,2,4\text{-triazole})_{0.5}]$. Protonation of the N-4 position precludes bridging between layers, while the bridging mode adopted by the N-1 and N-2 donors within a layer results in folding and the undulating profile of this two-dimensional oxide.

Acknowledgment. The work at Syracuse University was supported by NSF Grant CHE9617232. The work at North Carolina State University was supported by the U.S. Department of Energy, Office of Basic Sciences, Division of Materials Sciences, under Grant DE-FG05-86ER45259.

Supporting Information Available: Tables of atomic coordinates, isotropic and anisotropic thermal parameters, and bond lengths and angles for $[MoO_3(4,4'\text{-bpy})_{0.5}]$, $[H_xMoO_3(4,4'\text{-bpy})_{0.5}]$, and $[MoO_3(1,2,4\text{-trizaole})_{0.5}]$. This material is available free of charge via the Internet at http://pubs.acs.org.

IC000496L